Unusual ferromagnetic superexchange in $CdVO_3$: The role of Cd

Alexander A. Tsirlin,* Oleg Janson, and Helge Rosner†
Max Planck Institute for Chemical Physics of Solids, Nöthnitzer Str. 40, 01187 Dresden, Germany
(Received 8 April 2011; revised manuscript received 11 August 2011; published 31 October 2011)

A microscopic magnetic model of the low-pressure modification of $CdVO_3$ is established, based on density functional theory (DFT) band-structure calculations, magnetization measurements, and quantum Monte Carlo simulations. This compound is a rare example of a quasi-one-dimensional spin-1/2 system showing exclusively ferromagnetic exchange. The spin lattice of $CdVO_3$ entails zigzag chains with an effective intrachain coupling $J \simeq -90$ K and interchain couplings of $J_c \simeq -18$ K and $J_a \simeq -3$ K. Quantum fluctuations are partially suppressed by the sizable interchain coupling J_c that leads to an intermediate regime between one-dimensional and two-dimensional ferromagnetic systems. Apart from the peculiar spin model, $CdVO_3$ features an unusual mechanism of ferromagnetic superexchange. The couplings largely originate from Cd 5*s* states mediating hoppings between half-filled and empty 3*d* states of V^{+4}.

DOI: 10.1103/PhysRevB.84.144429 PACS number(s): 75.30.Et, 75.10.Jm, 75.50.Gg, 71.20.Ps

I. INTRODUCTION

Ferromagnetism and antiferromagnetism, the two opponent magnetic interactions, are rarely balanced, because specific mechanisms of the magnetic exchange tend to favor one of the two options. For example, itinerant systems are prone to ferromagnetic Stoner instabilities, whereas superexchange in magnetic insulators is a source of mostly antiferromagnetic (AFM) interactions.[1] This makes AFM ground states more common among insulating transition-metal compounds. Antiferromagnetism utterly dominates in low-dimensional magnets, where long-range and typically AFM couplings between the low-dimensional units (chains or layers) induce the overall AFM order. In particular, most of the quasi-one-dimensional (1D) spin-1/2 ferromagnetic-chain systems are antiferromagnetically ordered because the interchain couplings are AFM.[2–4] Low-dimensional spin-1/2 magnets with ferromagnetic (FM) ground state are still rare and restricted to systems based on organic radicals[5,6] or Cu^{+2} compounds with nontrivial orbital ordering.[7–9]

The aforementioned trend is violated by one peculiar compound, the low-pressure modification[10] of $CdVO_3$. Its 1D crystal structure (see Fig. 1),[11] featuring zigzag chains of edge-sharing VO_5 pyramids, seemingly represents an archetypal AFM insulator, where orbital degrees of freedom are eliminated by the square-pyramidal coordination of V^{+4}. The interchain couplings are long-range and likely AFM because of the underlying V-O-O-V superexchange pathways that typically lead to AFM couplings, while the FM superexchange is usually operative at short distances (see, e.g., Refs. 12–14). Moreover, the next-nearest-neighbor intrachain coupling J_2 between the corner-sharing vanadium pyramids should also be AFM, as in CaV_2O_5 and related compounds (see Sec. V and Table V).[15–17] However, experimental data disprove these empirical arguments, and reveal FM order in $CdVO_3$ below $T_C = 24$ K.[11] Magnetic susceptibility fitted with an expression for the classical FM chain model yields an effective intrachain coupling $J = -100$ K.[11] Dai *et al.*[18] found $J_1 \simeq -288$ K and $J_2 \simeq -90$ K from generalized gradient approximation (GGA) band structure calculations. They tentatively ascribed the unusual FM J_2 to the shift of the vanadium atom toward the base of the pyramid. However, their estimate of J_1 severely exceeds the experimental coupling of -100 K and, more importantly, does not address the nature of the interchain couplings, which are the driving force of the puzzling FM order in $CdVO_3$.

In the following, we explore the microscopic mechanism of ferromagnetism in $CdVO_3$ by extensive band structure calculations combined with magnetization measurements and quantum Monte Carlo (QMC) simulations. The application of diverse approaches for the evaluation of exchange couplings, along with the direct comparison to the experimental data, leads to a reliable microscopic magnetic model of $CdVO_3$. We show that the FM behavior of this compound is peculiar, and relate the ferromagnetism to Cd 5*s* orbitals mediating the FM superexchange. Below, the methodological part (Sec. II) is followed by band structure results in Sec. III and an analysis of the experimental data in Sec. IV. We conclude with a discussion and summary in Sec. V.

II. METHODS

The band structure was calculated within the framework of DFT using the full-potential local-orbital scheme (FPLO8.50-32).[19] We applied the local-density-approximation (LDA) with the Perdew-Wang parametrization[20] for the exchange-correlation potential. Exchange couplings were evaluated via two different procedures, a model approach and a supercell approach. In the former, the LDA band structure was mapped onto a multiorbital Hubbard model that was further treated perturbatively in the strongly correlated limit. In the supercell approach, the correlation effects in the V 3*d* shell were treated in a mean-field fashion by the LSDA + *U* method. Total energies for a number of collinear spin configurations were mapped onto a classical Heisenberg model to yield individual exchange couplings. Since the supercell approach led to somewhat puzzling results, we performed an extensive crosscheck using: (i) GGA[21] within FPLO; (ii) Vienna *ab initio* simulation package (VASP)[22] that performs projected augmented wave calculations and therefore employs a different basis set.[23] The energy cutoff was set to 400 eV. LDA results were obtained for the orthorhombic crystallographic unit cell, with a fine *k* mesh of 1040 points in the symmetry-irreducible

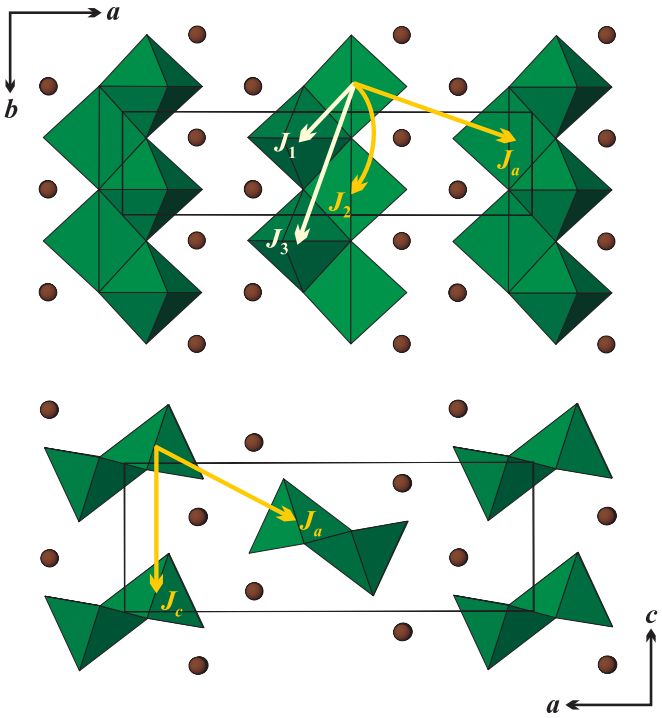

FIG. 1. (Color online) Crystal structure of $CdVO_3$ featuring zigzag chains of VO_5 pyramids. The chains are separated by Cd atoms (spheres).

part of the first Brillouin zone. DFT + U calculations utilized supercells doubled along b or c, with k meshes of 150–200 points.

To evaluate the magnetic susceptibility and Curie temperature of the proposed spin model, we performed QMC simulations using the `loop` algorithm[24] from the ALPS package.[25] 1D and two-dimensional (2D) finite lattices comprised $N = 120$ and 512 (32×16) sites, respectively, and ensured the absence of finite-size effects for the magnetic susceptibility within the temperature range under investigation. The Curie temperature was estimated from simulations for a three-dimensional (3D) model with different lattice sizes (see Sec. IV).

Experimental magnetization data were collected with a SQUID magnetometer (Quantum Design MPMS) in the temperature range 2–380 K in applied fields up to 5 T. The single-phase polycrystalline sample of $CdVO_3$ was prepared by a solid-state reaction of CdO and VO_2 in an evacuated silica tube at 700 °C for 24 hours. A 25% excess of CdO was introduced to compensate for the losses caused by the volatalization and reaction with the tube. The phase purity of the sample was checked by x-ray powder diffraction (Huber G670 Guinier camera, $CuK_{\alpha 1}$ radiation, image-plate detector, $2\theta = 3$–$100°$ angle range).

III. BAND STRUCTURE AND EXCHANGE COUPLINGS

A. LDA and model approach

The LDA band structure of $CdVO_3$ (see Fig. 2), with oxygen $2p$ valence bands below −3 eV and vanadium $3d$ bands at the Fermi level (E_F), is reminiscent of other V^{+4} oxides.[16,26] The contribution of cadmium is, however, larger than typical for an alkaline-earth (e.g., Ca^{+2}, Sr^{+2})[16,26] or even a d^{10} (e.g., Ag^{+1}, Zn^{+2})[27,28] cation. The bands below −8 eV originate from the filled Cd $4d$ orbitals, whereas the states at 3–4 eV show predominantly Cd $5s$ character. It is worth noting that the contributions of Cd and O at the Fermi level are comparable (6.2% and 9.6%, respectively, for $E \leqslant 0.2$ eV), yet oxygen $2p$ states dominate over Cd $5s$ between 1 and 3 eV. The sizable contribution at E_F distinguishes Cd from other cations that also produce conduction bands 3–4 eV above the Fermi level, but show a negligible contribution at E_F [for instance, Pb^{+2} in $PbZnVO(PO_4)_2$ (Ref. 28) or Se^{+4} in $VOSeO_3$ (Ref. 29)]. The obtained gapless energy spectrum originates from the underestimation of correlation effects in LDA. LSDA + U reproduces a band gap of about 2.0 eV ($U_d = 4$ eV, FPLO) in reasonable agreement with the brown color of $CdVO_3$.

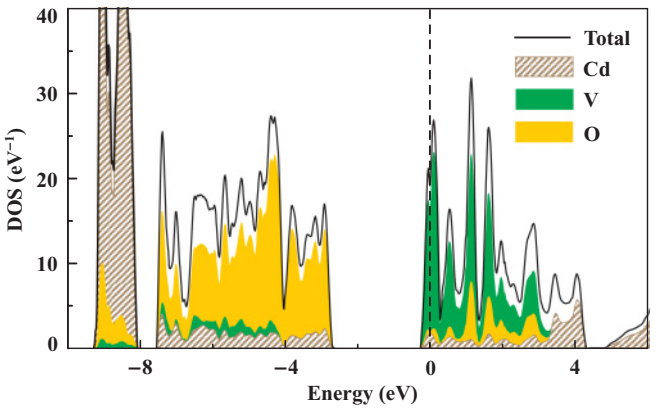

FIG. 2. (Color online) LDA density of states for $CdVO_3$. The Fermi level is at zero energy.

The band complex between −0.5 and 4.2 eV comprises 24 bands (see Fig. 3). Since there are four formula units per cell, these bands arise from six orbitals per formula unit: five V $3d$ and one Cd $5s$. The $3d$ levels of vanadium lie below the Cd states, and show a crystal-field splitting characteristic

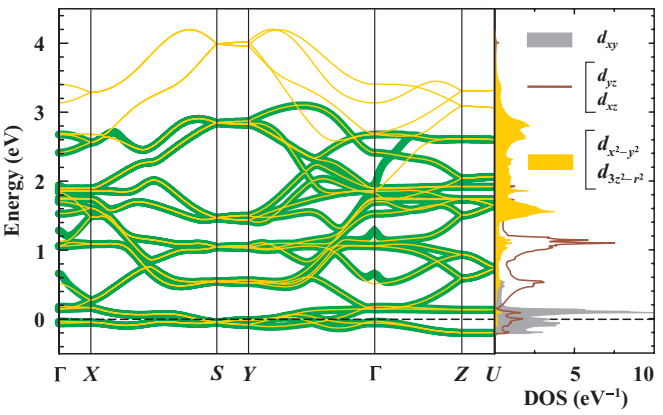

FIG. 3. (Color online) Left: LDA band structure for $CdVO_3$ (thin light lines) and the fit of the tight-binding model (thick dark lines) for the V $3d$-related bands. Right: orbital-resolved DOS for V $3d$ states. The Fermi level is at zero energy. The poor fit in the vicinity of the Γ point is related to the strong hybridization with the Cd $5s$ states represented by the four high-lying bands (not fitted). The notations of k points are Γ(0,0,0), X(0.5,0,0), S(0.5,0.5,0), Y(0,0.5,0), Z(0,0,0.5), and U(0.5,0,0.5).

of $V^{+4}O_5$ square pyramids.[30,31] Directing the z axis along the short (apical) V-O bond of the VO_5 pyramid, we find the lowest-lying d_{xy} crystal-field level, represented by four narrow bands at the Fermi level (see Fig. 3).

To analyze exchange couplings, we fit 20 vanadium bands[32] with a tight-binding model based on Wannier functions adapted to specific orbital symmetries,[33] and map the resulting transfer integrals t (hoppings)[34] onto a multiorbital Hubbard model with the effective on-site Coulomb repulsion $U_{\rm eff} = 4$ eV and Hund's coupling $J_{\rm eff} = 1$ eV.[12,35] In the $t \ll U_{\rm eff}$ limit, this model is reduced to the Kugel-Khomskii model, and the exchange couplings are expressed as follows:[36,37]

$$J = \frac{4t_{xy}^2}{U_{\rm eff}} - \sum_{\alpha} \frac{4t_{xy\to\alpha}^2 J_{\rm eff}}{(U_{\rm eff}+\Delta_\alpha)(U_{\rm eff}+\Delta_\alpha - J_{\rm eff})}, \qquad (1)$$

where t_{xy} and $t_{xy\to\alpha}$ are transfers between the xy states and from the xy (half-filled) to α (empty) states, respectively.[34] Δ_α stands for the crystal-field splitting between the xy and α states. Note that the states with a certain $3d$ orbital character and the resulting hoppings in Eq. (1) refer to Wannier functions centered on vanadium sites. Each Wannier function entails one of the vanadium $3d$ orbitals along with oxygen $2p$ and cadmium $5s$ states (Fig. 7). Therefore, metal–ligand transfers are implicitly contained in the hopping parameters t_i.

With Eq. (1), one evaluates full exchange couplings that are a sum of the AFM superexchange, arising from the transfers between the half-filled xy states [Eq. (1), first term], and the FM superexchange due to the hoppings to empty d states [Eq. (1), second term]. The efficiency of the LDA-based model approach has been demonstrated in Refs. 12, 28, and 35 providing a direct comparison to the experiment.

The leading exchange couplings calculated according to Eq. (1) are listed in Table I. The FM components of J_1 and J_2 surpass the AFM superexchange. The interchain coupling along c lacks any AFM component, yet there is a sizable FM contribution of -17 K. The interchain coupling along a is weaker but also FM. Further couplings are below 2 K (in terms of the absolute value) with an exception of $J_3 \simeq -8$ K, which is the third-neighbor intrachain coupling.

The exclusively FM couplings in $CdVO_3$ readily lead to the FM long-range order. Therefore, the results of the model approach are consistent with the experimental data, at least on the qualitative level. In Sec. IV, we will further demonstrate a good quantitative agreement with the experiment, while the rest of the present section is focused on the application of the supercell approach (Secs. III B and III C) and on the microscopic origin of ferromagnetism in $CdVO_3$ (Sec. III D).

TABLE I. Interatomic distances (in Å) in the $CdVO_3$ structure and the exchange couplings (in K) calculated with Eq. (1): the AFM ($J^{\rm AFM}$) and FM ($J^{\rm FM}$) contributions and the resulting total exchange (J).

	Distance	$J^{\rm AFM}$	$J^{\rm FM}$	J
J_1	3.05	18	−87	−69
J_2	3.60	21	−30	−9
J_3	5.93	0	−8	−8
J_c	5.20	0	−17	−17
J_a	5.79	1	−4	−3

B. DFT + U puzzles

The supercell approach to the evaluation of exchange couplings is based on LSDA + U (more generally, DFT + U) calculations that effectively reproduce the gapped energy spectrum of a Mott insulator. The DFT + U method rests upon the mean-field solution of the Hubbard model in the strongly correlated limit, but the incorporation of this solution into the self-consistent procedure leads to several features making the DFT + U results different from that of the perturbative treatment on top of LDA (model approach). One difference is the application of the onsite Coulomb repulsion and exchange to individual atomic-like orbitals in DFT + U instead of hybridized LDA bands (corresponding to molecular-like orbitals or Wannier functions) in the model approach. Therefore, the DFT + U parameters U_d and J_d are generally different from $U_{\rm eff}$ and $J_{\rm eff}$ in the Hubbard model.[38,39] The second feature is the double-counting-correction (DCC) scheme that subtracts part of the Coulomb energy already contained in LSDA, and enables the self-consistent procedure. Depending on the filling of individual d orbitals, the DCC is applied in either around-mean-field (AMF) or fully-localized-limit (FLL) fashions.

The choices of U_d, J_d, and the DCC are made on empirical grounds, and retain a certain ambiguity. Here, we focus on the previously overlooked effect of DCC, with U_d and J_d fixed at 3 and 1 eV, respectively. These values have been justified by FPLO LSDA + U calculations for several V^{+4} compounds.[12,30,35] We also varied U_d in the physically reasonable range of 2.5–6 eV, but no qualitative differences were found. To avoid calculations for large supercells, we estimated $J_1 + J_3$ instead of evaluating J_1 and J_3 separately. According to Table I, $|J_3| \ll |J_1|$, i.e., one may assume $J_1 + J_3 \simeq J_1$.

The AMF and FLL results for the exchange couplings in $CdVO_3$ are rather different (see Table II).[34] AMF evaluates the mostly antiferromagnetic scenario, while FLL renders J_1 strongly FM. We further checked these results against the different exchange-correlation potential (GGA + U) and the different band structure code. For a given DCC, the LSDA + U and GGA + U estimates closely match. The VASP calculations can be done for FLL only, and support the respective estimates from FPLO. A marginal difference between the FPLO and VASP

TABLE II. Exchange couplings (in K) evaluated by the DFT + U supercell procedure for different functionals, double-counting-correction (DCC) schemes, and band structure codes. The DFT + U parameters are set to $U_d = 3$ eV (FPLO), $U_d = 4$ eV (VASP), and $J_d = 1$ eV (both codes).

$J_1 + J_3$	J_2	J_a	J_c	Functional	DCC	Code
−17	21	2	9	LSDA + U	AMF	FPLO
−18	30	2	8	GGA + U	AMF	FPLO
−130	11	−4	−24	LSDA + U	FLL	FPLO
−117	17	−3	−17	GGA + U	FLL	FPLO
−122	−4	−3	−26	LSDA + U	FLL	VASP

results (especially for the second-neighbor coupling J_2) is related to different basis sets and, consequently, different projection schemes employed in the construction of the DFT + U occupation matrix. This difference also explains the 1 eV offset in the value of U_d (see Ref. 38). Another remark regards the GGA (without U) results by Dai *et al.*[18] who found both J_1 and J_2 FM, with a clearly overestimated absolute value of J_1. Their results cannot be directly compared to ours, because uncorrelated GGA calculations heavily underestimate correlation effects (for example, the reported band gap of about 0.5 eV[18] is much too small to explain the brown color of $CdVO_3$). The neglect of strong correlation effects typically leads to huge errors in the exchange couplings, as demonstrated, e.g., in Ref. 40.

Table II shows that the DFT + U estimates are robust with respect to the exchange-correlation potential and to the particular basis set employed in the band structure code. Thus, the problem stems from the choice of the DCC, which has a strong and unanticipated effect on the computed exchange couplings. A simple qualitative analysis identified the correct ground state for the FLL set of exchange parameters, whereas AMF predicts the wrong ground state. Indeed, the FM ground state in $CdVO_3$ requires FM interchain couplings J_a and J_c and the FM or weakly AFM J_2. The AFM next-nearest-neighbor intrachain coupling J_2 frustrates J_1, but does not break the FM ground state for $J_2/|J_1| < \frac{1}{4}$ (Ref. 41). The FLL results $J_a, J_c < 0$ and $J_2/|J_1| \leqslant 0.15$ fulfill both conditions. By contrast, $J_2/|J_1| \simeq 1$ obtained in AMF induces a spiral order along the chains that are further coupled antiferromagnetically. Therefore, the AMF-based scenario is unrealistic.

The above analysis puts forward the advantages of FLL in evaluating the exchange couplings for $CdVO_3$. This conclusion is reinforced by the physical meaning of different DCC schemes.[42] While AMF describes the regime of moderate correlations, FLL should be appropriate for strongly correlated systems ($t_i \ll U_{\text{eff}}$), such as $CdVO_3$. To check whether this DCC can be used universally, we calculated exchange couplings for several simple V^{+4} compounds and further explored the effect of the DCC on the stability of different magnetic states in DFT + U.

C. Double-counting correction: AMF versus FLL

To compare the performance of the AMF and FLL versions of DFT + U, we select five representative V^{+4} compounds showing chainlike magnetic behavior (see Table III). While details of the interchain couplings and the magnetic ground state may be different (and, in some cases, not fully understood), the AFM nature of the intrachain couplings is safely established experimentally.[26,43–46] The key difference between our test systems is the mutual arrangement of the vanadium polyhedra. To analyze the connectivity, we only consider the magnetic unit, a VO_5 square pyramid, despite that the actual crystallographic local environment is often described as an octahedron. The advantage of our description is the simple identification of the relevant superexchange pathway through the oxygen atoms lying in the basal plane of the pyramid. Since all systems under consideration reveal the d_{xy} orbital ground state, the axial oxygen atom neither connects the pyramids nor contributes to the superexchange, and only the oxygen atoms in the basal plane take part in the superexchange couplings.

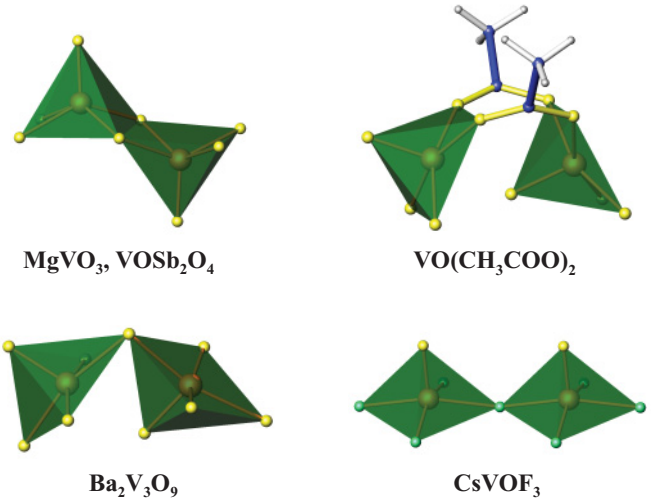

FIG. 4. (Color online) Superexchange pathways in the test compounds listed in Table III.

The test systems represent several different regimes (see Fig. 4): (i) edge-sharing VO_5 pyramids ($VOSb_2O_4$ and the low-pressure modification of $MgVO_3$),[43,44] (ii) corner-sharing VO_5 pyramids with either twisted ($Ba_2V_3O_9$, V-O-V angle of 96.4°)[26] or nearly linear ($CsVOF_3$, V-O-V angle of 164.9°)[45] geometries, and (iii) VO_5 pyramids bridged by a nonmagnetic acetate (CH_3COO^-) group.[46]

The intrachain exchange coupling J is evaluated as the energy difference between the FM and AFM spin configurations. Further couplings, both interchain and long-range intrachain, are rather weak and irrelevant for the present analysis. Quantitative estimates of these weak couplings and detailed structural information can be found in the preceding studies, where the exchange integrals were successfully evaluated using the model approach.[26,47–49]

In Table III, we compare AMF and FLL results for the leading intrachain exchange couplings. Here, we use $U_d = 3$ eV for five-fold-coordinated V^{+4} ($MgVO_3$, $VOSb_2O_4$), $U_d = 4$ eV for six-fold-coordinated V^{+4} ($Ba_2V_3O_9$, $CsVOF_3$, $VO(ac)_2$), and $J_d = 1$ eV for all test compounds. The octahedral oxygen environment requires a higher U_d, as shown in, e.g., Refs. 27 and 30. The corner-sharing ($Ba_2V_3O_9$, $CsVOF_3$) or indirect [$VO(CH_3COO)_2$] connections between the VO_5 pyramids lead to a remarkably small difference between AMF and FLL.

TABLE III. Test quasi-1D V^{+4} compounds, the V-V distances d (in Å), the connections between the VO_5 pyramids, and the exchange couplings J (in K) obtained from the AMF or FLL supercell calculations and from the experiment.

Compound	d(V-V)	Connection	J^{AMF}	J^{FLL}	J^{exp}	Refs.
$MgVO_3$	2.98	edge-sharing	128	−84	100	43
$VOSb_2O_4$	3.01	edge-sharing	248	154	250	44
$Ba_2V_3O_9$	3.01	corner-sharing	79	84	94	26
$CsVOF_3$	3.91	corner-sharing	143	157	132	45
$VO(CH_3COO)_2$	3.48	via acetate bridges	544	528	430	46

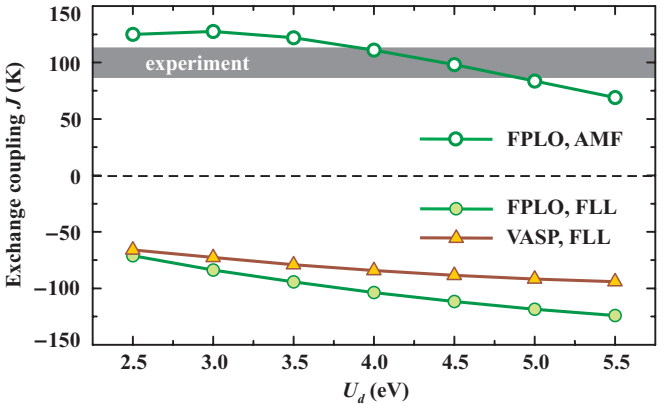

FIG. 5. (Color online) Intrachain exchange coupling in $MgVO_3$ calculated by LSDA + U for different values of Coulomb repulsion parameter U_d and different DCC schemes: AMF (open symbols) and FLL (filled symbols). The marginal difference between the FLL results obtained in FPLO and in VASP is likely related to the different basis sets.

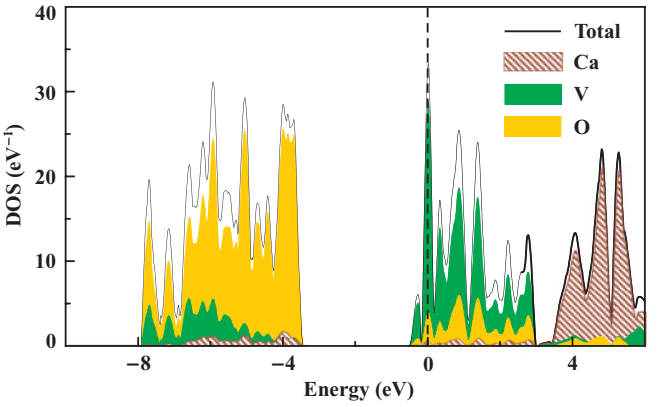

FIG. 6. (Color online) LDA density of states for the fictitious $CdVO_3$-type $CaVO_3$ (compare to Fig. 2). The Fermi level is at zero energy.

By contrast, there are large discrepancies for the couplings between edge-sharing pyramids, especially in $MgVO_3$. These discrepancies are basically independent of the U_d value, because J^{AMF} and J^{FLL} show similar evolution with a nearly constant offset of $J^{\mathrm{AMF}} - J^{\mathrm{FLL}} \simeq 100$ K in $VOSb_2O_4$ and about 200 K in $MgVO_3$ (see Fig. 5). In $VOSb_2O_4$, the discrepancy might be still tolerable, because both types of DCC yield the correct antiferromagnetic solution. The weaker exchange coupling, along with a larger offset between AMF and FLL, render the FLL result for $MgVO_3$ qualitatively wrong. Figure 5 shows that any reasonable value of U_d leads to negative J^{FLL} violating the experimental AFM coupling. The VASP calculations for $MgVO_3$ produce similar J values and confirm the intrinsic nature of the problem.

Based on our findings for the test compounds, we arrive at two conclusions that are—at this stage—rather empirical: (i) the particular choice of the DCC scheme is relevant for short-range couplings only; more specifically, only the couplings between the edge-sharing vanadium pyramids are affected, and (ii) for edge-sharing pyramids, neither DCC can be used universally, because FLL produces a realistic scenario for $CdVO_3$, while failing for $MgVO_3$, and in AMF the situation is exactly the opposite. We believe that the broad range of coupling geometries considered in our study makes this empirical conclusions a helpful guidance for future computational work on V^{+4} oxides and other transition-metal compounds. We also emphasize the remarkably good performance of the model approach for $CdVO_3$. The model approach is free from the double-counting problem, lacks any ambiguity, and represents an appealing alternative to the DFT + U supercell calculations. A further discussion of methodological aspects and tentative remarks on the possible origin of the DCC effects are given in Sec. V.

D. Origin of ferromagnetism

The FM behavior of $CdVO_3$ contrasts with the AFM properties of other V^{+4} compounds, such as quasi-1D $MgVO_3$ and $VOSb_2O_4$ or quasi-2D CaV_2O_5, CaV_3O_7, and CaV_4O_9. While J_1 is a nearly 90° and possibly FM V-O-V superexchange, the weakness of J_2 as well as the FM nature of J_a and J_c are less clear from a microscopic point of view. Dai *et al.*[18] claimed that the shift of the vanadium atom toward the basal plane of the VO_5 pyramid could cause FM J_2. However, they did not verify this conjecture, and refrained from any analysis of the FM interchain couplings, which are crucial for the FM long-range order. Here, we argue that the origin of ferromagnetism in $CdVO_3$ is different, and relates to the admixture of Cd states to the magnetic orbitals (Wannier functions). We justify this mechanism by considering a model system, a hypothetical $CaVO_3$ compound with the crystal structure of $CdVO_3$ but Ca occupying the Cd position. In our analysis, we follow the approach of Refs. 16, 28 and 30 that utilize the ability of DFT to evaluate microscopic parameters of fictitious compounds and, therefore, investigate the influence of different structural features on the magnetic properties.

The band structures of $CdVO_3$ and hypothetical $CaVO_3$ are rather similar, yet $CaVO_3$ is free from the low-lying Cd 5s bands (compare Figs. 2 and 6). Therefore, vanadium bands are largely mixing with O 2p and basically lack the cation contribution.[34] This change in the band structure has a strong effect on individual transfer integrals and the resulting

TABLE IV. Exchange couplings (in K) in the hypothetical $CaVO_3$ compound with the $CdVO_3$ structure. The J^{AFM}, J^{FM}, and $J = J^{\mathrm{AFM}} + J^{\mathrm{FM}}$ values are obtained from Eq. (1) (model approach), whereas the numbers in the last two columns (AMF and FLL) are calculated via the supercell approach with different DCC (LSDA + U, $U_d = 3$ eV, $J_d = 1$ eV). Similar to Table II, the LSDA + U estimates of J_1 are in fact $J_1 + J_3$ with $J_3 \simeq 5$ K according to the model analysis.

	Model approach			LSDA + U	
	J^{AFM}	J^{FM}	J	J AMF	J FLL
J_1	26	−42	−16	−28	−163
J_2	105	−23	82	133	83
J_c	0	0	0	1	−3
J_a	1	−1	0	2	−2

TABLE V. Exchange couplings between corner-sharing VO_5 pyramids: V-O-V angles (in deg), V-V distances (in Å), and exchange couplings J (in K) estimated from the experiment (marked with an asterisk) or DFT calculations.

Compound	α(V-O-V)	d(V-V)	J	Refs.
$Ba_2V_3O_9$	96.4	3.01	94*	26
MgV_2O_5	117.6	3.37	92	15
	141.1	3.69	144	15
CaV_4O_9	129.9	3.54	148	15
CaV_2O_5	132.9	3.49	608	15
	135.3	3.60	122	15
$CdVO_3$	136.1	3.60	<20	This work
$PbVO_3$	147.7	3.80	203*	27
$CsVOF_3$	164.9	3.91	132*	45

exchange couplings (see Table IV). Compared to Table I, we find (i) the increase in AFM J_2, (ii) the AFM nature of J_a and J_c, and (iii) equally strong interchain couplings ($J_a \simeq J_c$). The hypothetical $CaVO_3$ is predicted to be predominantly antiferromagnetic, and conforms to the trends established for V^{+4} compounds. Specifically, the long-range interchain couplings are AFM, whereas J_2 is about 100 K, as in MgV_2O_5 and CaV_4O_9 (see Sec. V and Table V).

The LSDA + U results for $CaVO_3$ reveal the same strong dependence on the DCC, as previously observed in $CdVO_3$ (compare Tables II and IV). The AMF and FLL calculations basically agree on the sizable AFM J_2, but strikingly differ in the estimate of the short-range coupling J_1. While we can not obtain any experimental information on the hypothetical $CaVO_3$ compound, it is instructive to compare the LSDA + U estimates of J_1 to the independent result from the model approach. The model estimate of $J_1 \simeq -16$ K is now in good agreement with the AMF prediction $J_1 \simeq -28$ K, while the FLL estimate of $J_1 \simeq -163$ K is far too large in terms of the absolute value. A further discussion of methodological problems related to the DCC of DFT + U is given in Sec. V.

The role of the Cd 5s states in the magnetism of $CdVO_3$ is elucidated by Wannier functions. In Fig. 7, we compare the V d_{xy}-based Wannier functions for $CdVO_3$ and $CaVO_3$. Apart from the leading V d_{xy} contributions, both Wannier functions involve oxygen p orbitals. In $CdVO_3$, there is an additional Cd 5s contribution, which is missing in $CaVO_3$.

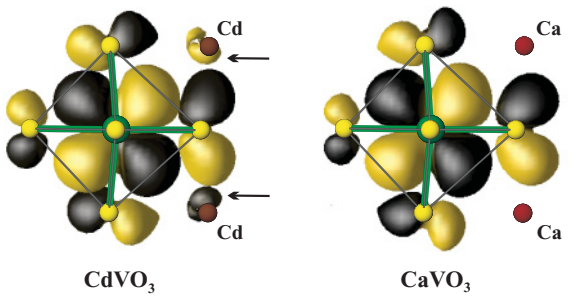

FIG. 7. (Color online) Vanadium d_{xy}-based Wannier functions for $CdVO_3$ (left) and hypothetical $CaVO_3$ (right). Note the Cd 5s contributions (marked with arrows) that are missing in the Ca-containing compound.

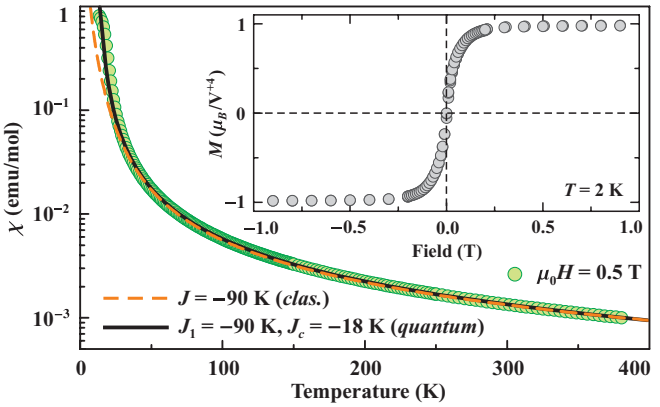

FIG. 8. (Color online) Magnetic susceptibility of $CdVO_3$ measured in an applied field of 0.5 T (filled circles) and the fits with the classical 1D model (dashed line) as well as the quantum 2D J_1-J_c model (solid line). Inset: magnetization curve at 2 K.

Similar features are found for Wannier functions based on empty vanadium orbitals. The Cd orbitals represent "tails" of the Wannier functions and amplify interorbital hoppings that drive the FM superexchange.

IV. ANALYSIS OF THE EXPERIMENTAL DATA

The magnetic susceptibility (χ) of $CdVO_3$ steeply increases from 380 to 2 K and clearly indicates the FM nature of the system (see Fig. 8). At low temperatures, the magnetization reaches the saturated value of about 1 μ_B at the applied field of less than 0.2 T. The lack of hysteresis may be related to a very weak anisotropy of V^{+4} (Ref. 50). Above 230 K, the susceptibility follows the Curie-Weiss law,

$$\chi = \chi_0 + \frac{C}{T+\theta}, \tag{2}$$

where $\chi_0 = -70 \times 10^{-6}$ emu/mol is the temperature-independent contribution of core diamagnetism and van Vleck paramagnetism, $C = 0.368$ emu K mol^{-1} is the Curie constant, and $\theta = -46$ K is the Weiss temperature. The C value corresponds to the effective magnetic moment of 1.70 μ_B that perfectly matches the expected value of $g\mu_B\sqrt{S(S+1)} = 1.697\ \mu_B$ with $g = 1.96$ from ESR.[11] The negative Weiss temperature is a signature of FM couplings leading to a positive deviation from the Curie-Weiss behavior below 230 K.

Onoda and Nishiguchi[11] fitted the magnetic susceptibility with the expression for the classical spin chain:[51]

$$\chi = \chi_0 + \frac{N_A g^2 \mu_B^2}{4k_B T}\frac{1+u}{1-u}, \quad u = \coth\left(-\frac{3J}{4T}\right) + \frac{4T}{3J}. \tag{3}$$

Our data can be described in a similar way ($\chi_0 = -70 \times 10^{-6}$ emu/mol, $g = 1.99$, $J = -90$ K, dashed line in Fig. 8), but the model itself does not apply to the spin-1/2 compound $CdVO_3$ because of inherent quantum fluctuations in low-dimensional spin-1/2 systems. For example, at $S = 1/2$, the classical AFM chain shows the susceptibility maximum at $T_{max}/J \simeq 0.35$, whereas for the quantum AFM chain, $T_{max}/J \simeq 0.64$. A pronounced difference should also be expected for the FM case. Indeed, the simulated curve for

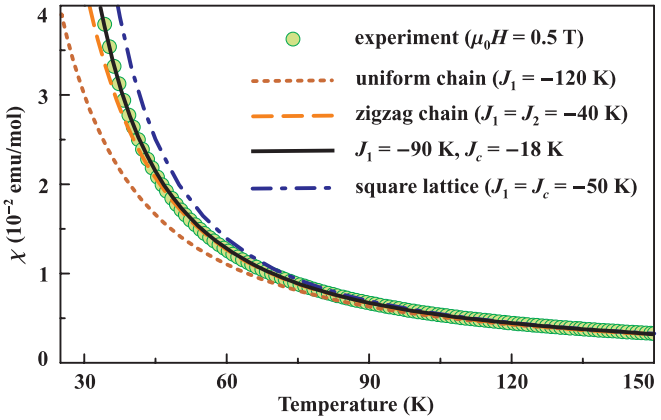

FIG. 9. (Color online) Fits of the magnetic susceptibility with different 1D and 2D spin models, see text for details.

the quantum FM chain ($J = -120$ K) fits our experimental data down to 100 K only (short-dashed line in Fig. 9). At lower temperatures, the 1D quantum model underestimates the susceptibility. This should be understood as an effect of quantum fluctuations that disturb the parallel alignment of spins and therefore reduce χ.

Since the experimental data for $CdVO_3$ conform to the classical model (see Fig. 8), quantum fluctuations in this compound are less pronounced than in the single quantum spin chain. This reduction could be related to the interchain coupling J_c that increases the dimensionality, or the FM intrachain coupling J_2 that increases the number of bonds at a lattice site without changing the dimensionality. We start with the first option, which is also favored by DFT since $|J_2| \ll |J_1|$. The 2D J_1-J_c model fits the experimental data down to 30 K with $J_1 = -90$ K, $J_c/J_1 = 0.2$, $g = 1.96$, and $\chi_0 = -80 \times 10^{-6}$ emu/mol (solid line in Fig. 9). For comparison, we also considered the isotropic 2D model (FM square lattice, $J_c = J_1 = -50$ K) where quantum fluctuations are further suppressed by the increased dimensionality. This model consequently overestimates the susceptibility below 90 K (dash-dotted line in the same figure). Therefore, $CdVO_3$ exhibits an intermediate regime between 1D and 2D FM systems.

The long-range FM order in $CdVO_3$ is stabilized by the interchain couplings J_a and J_c. To evaluate the Curie temperature T_C, we considered the 3D J_1-J_c-J_a spin model and calculated the Binder ratio of magnetization $B(T) = \langle m^4 \rangle / \langle m^2 \rangle^2$ for finite lattices of different size. The Curie temperature was determined as the crossing point of several $B(T)$ curves calculated for $L \times L/2 \times L/2$ finite lattices with $L \leqslant 64$. Similar to Refs. 52 and 53, we reduced the dimensions of the lattices along J_a and J_c to account for the anisotropic nature of our system. Using $J_a/J_1 = 0.03$ (Tables I and II), we arrive at $T_C/J_1 = 0.212$ ($T_C = 19$ K) that is slightly below the experimental value of 24 K. To reach the experimental Curie temperature, one has to take $J_a/J_1 = 0.07$ which is, however, inconsistent with the susceptibility fit. Since there are four couplings J_a and two coupling J_c at each lattice site, $J_a/J_1 = 0.07$ increases the overall energy of the interchain couplings by 70 %, and alters the susceptibility fit.

The marginal underestimate of T_C in the J_1-J_a-J_c model may be related to magnetic anisotropy, which lies beyond the scope of the present study, or the second-neighbor intrachain coupling J_2. According to DFT results, this coupling is either weakly FM (Table I) or weakly AFM (Table II). The AFM J_2 introduces frustration and disables the QMC techniques because of the sign problem. By contrast, the effect of FM J_2 can be readily evaluated. At weak FM J_2, the overall energy of the intrachain exchange (−90 K) is merely redistributed between J_1 and J_2. Using $J_1 = J_2 = -40$ K, we are able to introduce more significant changes by reducing quantum fluctuations and improving the susceptibility fit even within the purely 1D J_1-J_2 model (long-dashed line in Fig. 9). The second-neighbor coupling J_2 brings the system closer to the classical regime, thereby reducing the fitted interchain coupling. Since the ordering temperature is mostly sensitive to the value of J_c, the J_1-J_2-J_a-J_c model further underestimates T_C. Therefore, the sizable FM J_2 is unlikely. In conclusion, we argue that the unfrustrated J_1-J_a-J_c spin lattice, providing a remarkable fit of the susceptibility and a reasonable estimate of T_C, is a valid microscopic model of $CdVO_3$. This model strongly supports our computational results: compare the experimental $J_1 \simeq -90$ K, $J_a \simeq -3$ K, and $J_c \simeq -18$ K to the calculated $J_1 \simeq -69$ K, $J_a \simeq -3$ K, and $J_c \simeq -17$ K (Table I).

V. DISCUSSION AND SUMMARY

The peculiar ferromagnetism of $CdVO_3$ puts forward several important issues. First, we have demonstrated the importance of the DCC scheme as one of the delicate parameters of the DFT + U method. While it is usually difficult to make a well-justified choice of the DCC scheme, empirical recipes can be used, as we show below. We found that FLL produces accurate estimates for certain compounds, such as $CdVO_3$, but it may fail in closely related systems (e.g., $MgVO_3$) where AMF is, on the contrary, the method of choice. The most pragmatic and safe solution to this problem would be the adjustment of the DCC against the experimental data for each specific compound. While this does not diminish the crucial role of band structure calculations in the microscopic modeling of complex materials, the constant reference to the experimental data deprives computational methods of one important advantage, the ability to predict the magnetism of hitherto unexplored systems. To remedy this drawback, we performed a test study of several V^{+4} compounds with different coupling geometries.

Based on the comparative study in Sec. III C, we conclude that the ambiguity related to the choice of DCC is confined to short-range couplings only. Moreover, the uncertainty is only present for edge-sharing VO_5 pyramids in $MgVO_3$, $CdVO_3$, and $VOSb_2O_4$. The similarly short V-V distance of about 3.0 Å in $Ba_2V_3O_9$ with the corner-sharing pyramids does not cause any problems: both AMF and FLL results are in excellent agreement with the experiment (Table III). The principal difference between the edge-sharing and corner-sharing geometries is the combination of the direct V-V exchange and V-O-V superexchange in the former, while only the V-O-V superexchange is featured by the latter. It is the combination of the direct exchange and superexchange or

the direct exchange itself that are not well reproduced by DFT + U, presumably, due to the oversimplified mean-field treatment of correlation effects. The accurate results of the LDA-based model approach (Table I) ensure the high accuracy of the hopping parameters used as an input. Therefore, the underlying interatomic interactions are well reproduced even in LDA, but a better treatment of the onsite correlation effects is required. The development of the respective computational techniques will be a rewarding but challenging task that lies far beyond the scope of our study.

Presently, we are able to formulate the following recipes for calculating exchange couplings in transition-metal compounds. The conventional supercell approach (DFT + U calculations for different spin configurations) can be safely used for long-range couplings and even for short-range couplings not involving the direct overlap of the magnetic orbitals. In this case, the choice of the DCC plays a minor role compared to other factors, such as the adjustment of the Coulomb repulsion parameter U_d. Once the direct overlap of the magnetic orbitals is encountered, DFT + U results should be taken with caution and tested against experimental data or against independent computational estimates. Particularly, we put forward the model approach as an appealing alternative to the DFT + U calculations. The perturbative treatment of the multiorbital Hubbard model is based on the reliable LDA input, free from ambiguity, and uncovers individual hopping processes that are responsible for the superexchange. We believe that the combination of the model and supercell approaches is a viable and reliable tool for studying magnetic systems, as demonstrated by our present work on $CdVO_3$.

After commenting on the methodological aspects, we discuss the physics of $CdVO_3$. The unexpected FM behavior of this compound originates from Cd 5s states mediating the hoppings between the half-filled and empty states of V^{+4}. The interaction is, therefore, a superexchange, but its mechanism is different from the conventional orbital ordering scenario.[8,36] The orbital ordering induces magnetic (half-filled) orbitals of different symmetry on the neighboring atoms, and favors the hoppings between the half-filled and empty orbitals of the same symmetry. In $CdVO_3$, there is only one type of the magnetic orbital, hence ferromagnetism is driven by hoppings between orbitals of different symmetry.

The effect of Cd is easily recognized in Table V that compares exchange couplings between the corner-sharing VO_5 pyramids. Although one generally expects the increase in the AFM superexchange at V-O-V angles close to 180°, this trend does not hold for V^{+4} compounds due to the relevance of other structural features. For example, basal planes of the pyramids coincide in CaV_2O_5 and $CsVOF_3$, but remain nearly perpendicular in $Ba_2V_3O_9$ (see Fig. 4). This explains the broad range of possible V-O-V angles and their weak effect on the superexchange. The only general trend is the AFM nature of the coupling between the corner-sharing VO_5 pyramids. The couplings typically range between 100 and 200 K, and always exceed 90 K. $CdVO_3$ is a remarkable exception, with the AFM coupling reduced below 20 K because of the Cd 5s orbitals altering the superexchange.

The cation-mediated superexchange in vanadium oxides is not restricted to $CdVO_3$. For example, the unusually strong and frustrating second-neighbor exchange in $PbVO_3$ is likely driven by Pb 6p orbitals that marginally contribute to the V d_{xy} bands.[40] To verify the role of Pb in $PbVO_3$, we evaluated the second-neighbor coupling J_2 in the fictitious $SrVO_3$ having the tetragonal $PbVO_3$ structure. The calculations yield $J_2 = 24$ K in $SrVO_3$ against $J_2 = 69$ K in $PbVO_3$. A similar "diagonal" superexchange has been proposed for $Pb_{0.55}Cd_{0.45}V_2O_5$, although the intrinsic disorder of Pb and Cd atoms in this compound hampered an accurate experimental estimate of the respective coupling.[54] The aforementioned systems are, however, different from $CdVO_3$, because the Pb and Cd cations mediate an AFM superexchange. The nonmagnetic cations may have diverse effects on the superexchange, and the specific scenario is actually determined by the hybridization between the cation orbitals and oxygen orbitals entering vanadium-based Wannier functions. In many systems (e.g., vanadium phosphates[30]), there is no effect at all because the cation states are expelled from the Fermi level. The cation-mediated superexchange is not ubiquitous and requires specific coupling geometries, but it can be expected for a variety of cations featuring empty s (e.g., Zn^{+2}, Cu^{+1}, Ag^{+1}) or p (e.g., Bi^{+3}, Sn^{+2}) states closely above the Fermi level (see also Ref. 55). Respective compounds are likely to host nontrivial spin lattices and unusual magnetism.

Finally, we note that $CdVO_3$ is interesting on its own as a system showing an intermediate regime between the 1D and 2D ferromagnets. Experimental studies of FM uniform chains helped to find appropriate theoretical tools for solving the Heisenberg model in 1D, and disclosed peculiar soliton-type excitations.[56,57] The respective systems are close to the 1D limit, whereas the opposite, 2D limit is realized in K_2CuF_4 and related Cu^{+2} halides with layered perovskite-type structures.[7–9] $CdVO_3$ could be a reference point between these two qualitatively different model regimes that represent the ground states with zero (1D) and nonzero (2D) ordered magnetic moment. The crossover between the 1D and 2D regimes is rather well studied for the AFM case,[52] yet a comparative study of the FM case could be insightful.

In summary, we have developed a microscopic magnetic model of $CdVO_3$, and found out the origin of ferromagnetism in this compound. We argue that $CdVO_3$ is a ferromagnetic spin chain system with an effective (and mostly nearest-neighbor) intrachain coupling of −90 K and a sizable interchain coupling $J_c = -18$ K along one of the dimensions. Our model is based on extensive band structure calculations and verified by a direct comparison to the experimental magnetic susceptibility and Curie temperature. The unusual ferromagnetic couplings arise from Cd 5s orbitals that contribute to the vanadium-based Wannier functions, mediate hoppings between the half-filled and empty d states of vanadium, and lead to the ferromagnetic superexchange. This mechanism puts forward diverse effects of nonmagnetic cations on superexchange in transition-metal compounds.

ACKNOWLEDGMENTS

We are grateful to Yurii Prots and Horst Borrmann for x-ray diffraction measurements. A.T. was supported by Alexander von Humboldt foundation.

*altsirlin@gmail.com
†Helge.Rosner@cpfs.mpg.de

[1] P. W. Anderson, Solid State Phys. **14**, 99 (1963).
[2] C. P. Landee and R. D. Willett, Phys. Rev. Lett. **43**, 463 (1979); C. Dupas, J. P. Renard, J. Seiden, and A. Cheikh-Rouhou, Phys. Rev. B **25**, 3261 (1982).
[3] D. D. Swank, C. P. Landee, and R. D. Willett, Phys. Rev. B **20**, 2154 (1979).
[4] R. D. Willett, C. P. Landee, R. M. Gaura, D. D. Swank, H. A. Groenendijk, and A. J. van Duyneveldt, J. Magn. Magn. Mater. **15-18**, 1055 (1980); R. Hoogerbeets, E. H. Abu Bakr, and A. J. van Duyneveldt, Physica B **128**, 161 (1985).
[5] M. Takahashi, P. Turek, Y. Nakazawa, M. Tamura, K. Nozawa, D. Shiomi, M. Ishikawa, and M. Kinoshita, Phys. Rev. Lett. **67**, 746 (1991); Y. Nakazawa, M. Tamura, N. Shirakawa, D. Shiomi, M. Takahashi, M. Kinoshita, and M. Ishikawa, Phys. Rev. B **46**, 8906 (1992).
[6] K. Shimizu, T. Gotohda, T. Matsushita, N. Wada, W. Fujita, K. Awaga, Y. Saiga, and D. S. Hirashima, Phys. Rev. B **74**, 172413 (2006).
[7] I. Yamada, J. Phys. Soc. Jpn. **33**, 979 (1972); Y. Ito and J. Akimitsu, *ibid.* **40**, 1333 (1976).
[8] D. I. Khomskii and K. I. Kugel, Solid State Commun. **13**, 763 (1973).
[9] L. J. de Jongh, Physica B+C **82**, 247 (1976); R. Willett, H. Place, and M. Middleton, J. Amer. Chem. Soc. **110**, 8639 (1988), and references therein.
[10] Throughout the paper, we refer to the low-pressure modification of $CdVO_3$. The high-pressure phase has a perovskite-type structure and exhibits metallic behavior [B. L. Chamberland and P. S. Danielson, J. Solid State Chem. **10**, 249 (1974)].
[11] M. Onoda and N. Nishiguchi, J. Phys. Condens. Matter **11**, 749 (1999).
[12] A. A. Tsirlin and H. Rosner, Phys. Rev. B **83**, 064415 (2011).
[13] R. Nath, A. A. Tsirlin, E. E. Kaul, M. Baenitz, N. Büttgen, C. Geibel, and H. Rosner, Phys. Rev. B **78**, 024418 (2008).
[14] A. Rodríguez-Fortea, M. Llunell, P. Alemany, and E. Canadell, Phys. Rev. B **82**, 134416 (2010).
[15] M. A. Korotin, I. S. Elfimov, V. I. Anisimov, M. Troyer, and D. I. Khomskii, Phys. Rev. Lett. **83**, 1387 (1999).
[16] M. A. Korotin, V. I. Anisimov, T. Saha-Dasgupta, and I. Dasgupta, J. Phys. Condens. Matter **12**, 113 (2000).
[17] W. E. Pickett, Phys. Rev. Lett. **79**, 1746 (1997).
[18] D. Dai, H.-J. Koo, and M.-H. Whangbo, J. Solid State Chem. **175**, 341 (2003).
[19] K. Koepernik and H. Eschrig, Phys. Rev. B **59**, 1743 (1999).
[20] J. P. Perdew and Y. Wang, Phys. Rev. B **45**, 13244 (1992).
[21] J. P. Perdew, K. Burke, and M. Ernzerhof, Phys. Rev. Lett. **77**, 3865 (1996).
[22] G. Kresse and J. Furthmüller, Comput. Mater. Sci. **6**, 15 (1996); Phys. Rev. B **54**, 11169 (1996).
[23] P. E. Blöchl, Phys. Rev. B **50**, 17953 (1994); G. Kresse and D. Joubert, *ibid.* **59**, 1758 (1999).
[24] S. Todo and K. Kato, Phys. Rev. Lett. **87**, 047203 (2001).
[25] A. Albuquerque, F. Alet, P. Corboz, P. Dayal, A. Feiguin, S. Fuchs, L. Gamper, E. Gull, S. Gürtler, A. Honecker, R. Igarashi, M. Körner, A. Kozhevnikov, A. Läuchli, S. R. Manmana, M. Matsumoto, I. P. McCulloch, F. Michel, R. M. Noack, G. Pawłowski, L. Pollet, T. Pruschke, U. Schollwöck, S. Todo, S. Trebst, M. Troyer, P. Werner, and S. Wessel, J. Magn. Magn. Mater. **310**, 1187 (2007).
[26] E. E. Kaul, H. Rosner, V. Yushankhai, J. Sichelschmidt, R. V. Shpanchenko, and C. Geibel, Phys. Rev. B **67**, 174417 (2003).
[27] A. A. Tsirlin, R. Nath, C. Geibel, and H. Rosner, Phys. Rev. B **77**, 104436 (2008).
[28] A. A. Tsirlin, R. Nath, A. M. Abakumov, R. V. Shpanchenko, C. Geibel, and H. Rosner, Phys. Rev. B **81**, 174424 (2010).
[29] S.-H. Kim, P. S. Halasyamani, B. C. Melot, R. Seshadri, M. A. Green, A. S. Sefat, and D. Mandrus, Chem. Mater. **22**, 5074 (2010).
[30] A. A. Tsirlin and H. Rosner, Phys. Rev. B **79**, 214417 (2009).
[31] R. Valentí, T. Saha-Dasgupta, and F. Mila, Phys. Rev. B **68**, 024411 (2003).
[32] The fit is complicated by the substantial hybridization between V 3*d* and Cd 5*s* states. Since the ambiguity of the fit could affect the hopping parameters and thus the resulting exchange integrals, we carefully tested our estimates by varying energy windows for Wannier functions or adding explicit contributions of Cd 5*s* orbitals as "tails." We also constructed a 24-band model including Wannier functions with Cd 5*s* character. All these tests produced rather similar results and confirmed our main conclusion on the FM superexchange in $CdVO_3$.
[33] H. Eschrig and K. Koepernik, Phys. Rev. B **80**, 104503 (2009).
[34] See Supplemental Material at http://link.aps.org/supplemental/10.1103/PhysRevB.84.144429 for individual hopping parameters and DFT + U energy spectra.
[35] A. A. Tsirlin, R. Nath, J. Sichelschmidt, Y. Skourski, C. Geibel, and H. Rosner, Phys. Rev. B **83**, 144412 (2011).
[36] K. I. Kugel and D. I. Khomskii, Sov. Phys. Usp. **25**, 231 (1982).
[37] V. V. Mazurenko, F. Mila, and V. I. Anisimov, Phys. Rev. B **73**, 014418 (2006).
[38] A. A. Tsirlin, O. Janson, and H. Rosner, Phys. Rev. B **82**, 144416 (2010) and references therein.
[39] V. V. Mazurenko, S. L. Skornyakov, A. V. Kozhevnikov, F. Mila, and V. I. Anisimov, Phys. Rev. B **75**, 224408 (2007); V. V. Mazurenko, S. L. Skornyakov, V. I. Anisimov, and F. Mila, *ibid.* **78**, 195110 (2008).
[40] A. A. Tsirlin, A. A. Belik, R. V. Shpanchenko, E. V. Antipov, E. Takayama-Muromachi, and H. Rosner, Phys. Rev. B **77**, 092402 (2008).
[41] R. Zinke, S.-L. Drechsler, and J. Richter, Phys. Rev. B **79**, 094425 (2009).
[42] E. R. Ylvisaker, W. E. Pickett, and K. Koepernik, Phys. Rev. B **79**, 035103 (2009) and references therein.
[43] J. Choukroun, V. A. Pashchenko, Y. Ksari, J. Y. Henry, F. Mila, P. Millet, P. Monod, A. Stepanov, J. Dumas, and R. Buder, Eur. Phys. J. B **14**, 655 (2000).
[44] V. A. Pashchenko, A. Sulpice, F. Mila, P. Millet, A. Stepanov, and P. Wyder, Eur. Phys. J. B **21**, 473 (2001).
[45] D. W. Aldous, R. J. Goff, J. P. Attfield, and P. Lightfoot, Inorg. Chem. **46**, 1277 (2007).
[46] C. Weeks, Y. Song, M. Suzuki, N. A. Chernova, P. Y. Zavalij, and M. S. Whittingham, J. Mater. Chem. **13**, 1420 (2003).
[47] I. Chaplygin, R. Hayn, and K. Koepernik, Phys. Rev. B **60**, R12557 (1999).
[48] I. Chaplygin and R. Hayn, Phys. Rev. B **70**, 064510 (2004).
[49] H.-J. Koo and M.-H. Whangbo, Solid State Sci. **12**, 685 (2010).
[50] V. Gnezdilov, P. Lemmens, A. A. Zvyagin, V. O. Cheranovskii, K. Lamonova, Y. G. Pashkevich, R. K. Kremer, and H. Berger, Phys. Rev. B **78**, 184407 (2008).

[51]M. E. Fisher, Am. J. Phys. **32**, 343 (1964).
[52]A. W. Sandvik, Phys. Rev. Lett. **83**, 3069 (1999).
[53]P. Sengupta, C. D. Batista, R. D. McDonald, S. Cox, J. Singleton, L. Huang, T. P. Papageorgiou, O. Ignatchik, T. Herrmannsdörfer, J. L. Manson, J. A. Schlueter, K. A. Funk, and J. Wosnitza, Phys. Rev. B **79**, 060409(R) (2009).
[54]A. A. Tsirlin, R. V. Shpanchenko, E. V. Antipov, C. Bougerol, J. Hadermann, G. Van Tendeloo, W. Schnelle, and H. Rosner, Phys. Rev. B **76**, 104429 (2007).
[55]W. Geertsma and D. Khomskii, Phys. Rev. B **54**, 3011 (1996).
[56]K. Kopinga, T. Delica, and H. Leschke, Phys. Rev. B **40**, 7239 (1989); L. S. Campana, A. Caramico D'Auria, U. Esposito, and G. Kamieniarz, *ibid.* **41**, 6733 (1990); K. Kopinga, T. Delica, H. Leschke, and I. Riedel, *ibid.* **47**, 5447 (1993).
[57]K. Kopinga, A. M. C. Tinus, W. J. M. de Jonge, and G. C. de Vries, Phys. Rev. B **36**, 5398 (1987); G. C. de Vries, E. Frikkee, K. Kakurai, M. Steiner, B. Dorner, K. Kopinga, and W. J. M. de Jonge, *ibid.* **40**, 7011 (1989).